Corrado Baratti, MD
Alan S. Barnett, PhD
Carlo Pierpaoli, MD, PhD

Index terms:
Animals
Brain, growth and development, 10.91, 10.99
Brain, MR, 10.121411, 10.121413, 10.12146
Magnetic resonance (MR), relaxometry, 10.12146

Radiology 1999; 210:133–142

Abbreviations:
GM = gray matter
ROI = region of interest
Trace(**D**) = trace of the diffusion tensor
WM = white matter

[1] From the Neuroimaging Branch, National Institutes of Neurological Disorders and Stroke, National Institutes of Health, Bldg 10, Rm 4N252, 10 Center Dr, Bethesda, MD 20892-2289. Received February 23, 1998; revision requested April 15; final revision received August 4; accepted August 11. **Address reprint requests to** C.P.

© RSNA, 1999

Author contributions:
Guarantors of integrity of entire study, C.B., A.S.B., C.P.; study concepts and design, C.P.; definition of intellectual content, C B , A.S.B., C.P.; literature research, C.B.; experimental studies, C.B., A.S.B., C.P.; data acquisition, C.B.; data analysis, C.B., A.S.B., C.P.; statistical analysis, C.P.; manuscript preparation, editing, and review, C.B., A.S.B., C.P.

Comparative MR Imaging Study of Brain Maturation in Kittens with T1, T2, and the Trace of the Diffusion Tensor[1]

PURPOSE: To assess the time-course of the relaxation times and the orientationally averaged water diffusion coefficient D_{oav} in postnatal brain development.

MATERIALS AND METHODS: Multisection maps of T1, T2, and the trace of the diffusion tensor (Trace[**D**] = 3 × D_{oav}) were obtained in four kittens at eight time points.

RESULTS: In the adult, D_{oav} was about 700 μm²/sec in both white and gray matter. In the newborn, D_{oav} was 1,100–1,350 μm²/sec in white matter and 1,000 μm²/sec in gray matter. For all anatomic regions and time points, the correlation between D_{oav} and 1/T2 was high (R^2 = 0.87, $P \ll .001$). T1 showed a lower correlation with D_{oav} and a higher sensitivity to myelinization than did T2.

CONCLUSION: Although D_{oav} shows dramatic changes in the maturing brain, the high correlation between D_{oav} and T2 indicates that little additional information can be obtained by measuring this diffusion parameter during normal brain development. This contrasts with previous findings in brain ischemia, where D_{oav} and T2 appear to be uncorrelated. After including the authors' data and published iontophoretic measurements in a simple model of diffusion in tissues, the authors suggest that the underlying mechanisms of D_{oav} reduction in brain maturation and ischemia are different. D_{oav} changes during development are mainly affected by events occurring in the cellular compartment, while changes in extracellular volume fraction and tortuosity, which are thought to determine the reduction in D_{oav} during ischemia, are probably of secondary importance.

T1-weighted and T2-weighted magnetic resonance (MR) images are widely used for the clinical monitoring of brain development. The usefulness of conventional MR imaging is reliant on its superb depiction of gross brain anatomy and on its ability to aid in discrimination between white matter (WM) and gray matter (GM) at different stages of brain maturation (1). In addition to the magnetic relaxation properties of tissues, MR imaging methods can also be used to measure molecular diffusion (2). The ability of diffusion MR imaging to depict brain ischemia very early after onset, when conventional MR imaging findings would still be normal (3), has fueled expectations that diffusion MR imaging could also provide additional clinically relevant information about other pathologic and physiologic conditions, including brain development.

Previous diffusion MR imaging studies (4–6) of brain development have demonstrated that the apparent diffusion coefficient of water molecules decreases during brain maturation. Some authors (4,5) have also suggested that diffusion-weighted MR images are more sensitive than T1-weighted images for the detection of the onset of myelinization. When investigating anisotropic tissues such as WM, however, both diffusion-weighted images and apparent-diffusion-coefficient maps not only reflect intrinsic properties of the tissue but also are affected by the subject's orientation in the magnet. For this reason, diffusion-weighted images and apparent diffusion coefficient maps are difficult to interpret and cannot be used for the quantitative characterization of water diffusion in WM (7). Scalar quantities derived from the diffusion tensor, such as the trace of the diffusion tensor

(Trace[**D**]), do not present this problem (8). Trace(**D**) is equal to three times the orientationally averaged water diffusion coefficient D_{oav}, which represents the mean value of the diffusion coefficients measured in all possible directions. Trace(**D**) has similar values in the WM and GM in the brains of adult cats (9), monkeys (7), and humans (10,11).

The goals of this work were (*a*) to measure the time course of Trace(**D**) in different WM and GM regions during postnatal brain development in normal cats and (*b*) to study the correlation between Trace(**D**) and T1 and T2 to establish whether Trace(**D**) provides information unavailable with conventional, relaxometry-based MR imaging.

MATERIALS AND METHODS

Animal Model

Four kittens (two siblings from two litters, three male kittens and one female kitten) were studied with serial MR imaging of the brain under a protocol approved by the animal care and use committee of our institution. Cats were preferred over rodents, because the cat brain size is appropriate for the image resolution used and because rodents are lissencephalic animals whose gross brain anatomy is very different from that of humans. In addition, feline postnatal neurologic development resembles that of humans, although its timing is obviously different (12).

Each animal underwent eight serial MR imaging studies. The first study was performed on the 2nd or 3rd day after birth. The subsequent studies were performed weekly during the 1st month of life, biweekly during the 2nd month, and once at the ages of 3 and 4 months. Animals older than 4 months were not studied because WM myelinization, which is the latest event in brain development (13), is almost completed in 3-month-old kittens (14). Two adult cats were also imaged to obtain reference measures in a completely developed brain.

The animals were anesthetized with 1.5% isoflurane (Abbott Laboratories, North Chicago, Ill) during the MR imaging session, which lasted 1 hour 23 minutes for the diffusion-weighted acquisition, 21 minutes for T2 mapping, and 53 minutes for T1 mapping. Rectal temperature was continuously monitored with a fiberoptic thermometer and was maintained at 36.5°C–37.5°C with a water-heated pad. Kittens younger than 2 months were allowed to breathe spontaneously, and their respiratory frequency was monitored with a plethysmograph positioned around the chest. Older animals were intubated and mechanically ventilated to maintain expiratory carbon dioxide pressure at 38–40 mm Hg.

MR Imaging

We performed all MR imaging with a 2-T MR animal system (Omega; GE NMR Instruments, Fremont, Calif) equipped with self-shielded gradient coils capable of producing a maximum gradient strength of 40 mT/m. We used two home-built quadrature ''birdcage'' radio-frequency coils. One coil, used for kittens younger than 2 months, had an inner diameter of 39 mm. The other coil, used for kittens older than 2 months and for the adult cats, had an inner diameter of 62 mm.

Each MR imaging session consisted of three series: a set of 31 diffusion-weighted images for calculating the diffusion tensor, a four-echo Carr-Purcell-Meiboom-Gill sequence for calculating T2 maps, and five inversion-recovery spin-echo images for calculating T1 maps.

At each time point and for all techniques, we obtained eight coronal sections of the brain with the same section thickness, intersection gap, in-plane resolution, and field of view. These parameters, however, were set to different values that were dependent on the coil used and the age of the kitten. Section thickness was 1.2–2.0 mm, the intersection gap was 3.0–4.0 mm, and the field of view was 50–60 mm. The in-plane resolution was 128 × 128 at all time points. Given these parameters, the voxel size ranged from 0.18 mm^3 in newborns and young kittens to 0.44 mm^3 in older kittens and adult cats.

Diffusion-weighted MR imaging.—We acquired diffusion-weighted images with an interleaved echo-planar imaging sequence (15) that included a navigator echo for correction of motion artifacts. In addition to a non–diffusion-weighted image, we obtained images with five diffusion gradient strengths in six directions (11), which yielded values for the b-matrix trace that were equally spaced between 0 and 1,100 mm^2/sec. The image acquisition parameters were as follows: 5,000/76 (repetition time msec/echo time msec), no cardiac gating, 16 interleaves (eight echoes per interleaf), and trapezoidal diffusion gradients with 15-msec duration, ramp time of 0.4 msec, and center-to-center separation of 36.5 msec. After image reconstruction, we computed the b matrix (16) numerically for each image. We calculated the diffusion tensor **D** in each voxel according to the method of Basser et al (8,17) and generated maps of Trace(**D**) for each section by summing the three eigenvalues of **D** in each voxel.

T2 mapping.—We measured T2 by using a multiecho, multisection Carr-Purcell-Meiboom-Gill sequence similar to the one described by Mulkern et al (18), with the acquisition of eight sections with four echoes per section (repetition time = 5,000 msec, echo times = 50, 100, 150, 200 msec). We were unable to acquire more than four echoes per section due to hardware limitations. T2 was computed on a pixel-by-pixel basis from best-fit values of the slope of the log of the signal intensity versus echo time. In determining the best fit, we weighted each point by the square of its magnitude (see Bevington [19]).

T1 mapping.—We measured T1 by using a series of complex inversion-recovery images (repetition time = 5,000 msec, echo time = 19 msec, inversion times = 200, 400, 800, 1600, ∞ msec, where the inversion time = ∞ msec corresponds to an image acquired with no inversion pulse). We removed the polar ambiguity by using the image obtained with an inversion time of ∞ msec as a reference. We then computed T1 from the slope of log([signal in the reference image] − [signal in image obtained with inversion time TI]) versus the inversion time. This method involves only a linear least-squares fit and is therefore quite robust.

Phantom Study

It is well known that the acquisition of accurate measurements of T2 with a multisection imaging sequence may be problematic (20). To verify the accuracy of the T2 values measured with our imaging sequence, we prepared eight gelatin phantoms with different concentrations of dysprosium chloride (Sigma, St Louis, Mo), adjusted to provide a T2 in the range of 25–175 msec. Accurate T2 values for the phantom were obtained with a spectroscopic 32-echo Carr-Purcell-Meiboom-Gill sequence performed with the same MR imaging unit used for the animal study. The same phantoms were then imaged with the imaging sequence used for the animal study, and the T2 values were measured in regions of interest (ROIs) drawn on the computer-generated T2 maps. We computed the percent error of the imaging-measured T2 by using the spectroscopically-measured T2 as a reference.

ROI Analysis

We drew anatomic ROIs on the T1, T2, and Trace(**D**) maps by using the manual tracking system provided in IDL (ITERATIVE DATA LANGUAGE; Research Systems, Boulder, Colo). Five anatomic structures were selected: cortical GM, the caudate nucleus, the internal capsule, the corpus callosum, and subcortical WM. For each anatomic structure except the corpus callosum, we measured multiple ROIs positioned on both cerebral hemispheres and on at least two sections. To avoid partial volume averaging from adjacent cerebrospinal fluid, a single ROI was drawn in the corpus callosum on the section that contained its thickest portion. The reported mean value of each parameter in each anatomic structure is the average of all measurements obtained in multiple ROIs, weighted by the number of voxels in each ROI.

Statistical Analysis

We examined the degrees of correlation between 1/T1 and 1/T2, Trace(**D**) and 1/T1, and Trace(**D**) and 1/T2. We also computed correlation coefficients for the entire data set and for each anatomic ROI. Two parameters were considered to be significantly correlated if the regression coefficient was different from zero with a P value of less than .01. Two anatomic ROIs were considered to be different if the 95% CI of the slope and/or the intercept of their respective regression lines did not overlap.

RESULTS

In general, the lengthy MR procedure was well tolerated, even by the newborn kittens. It should be noted, however, that the younger animals were not mechanically ventilated; therefore, any prolonged apnea in those animals was potentially life-threatening. When a prolonged apnea occurred, we immediately removed the animal from the magnet; in some cases, we did not have enough time to repeat the examination. Of the 32 studies planned (four kittens imaged at eight time points), we were unable to obtain data in one diffusion tensor study, five T1 studies, and eight T2 studies. The first study after birth and the study at the 3rd week were completed for all parameters in only two animals. Studies at all other time points were completed in at least three animals. No new animals were added to those initially planned, because, for the purpose of testing the correlation between parameters, the statistical robustness of our data set proved to be high despite the missing data. All correlations tested had a high level of significance for the regression coefficient ($P \ll .001$), much higher than the level that we set for statistical significance (ie, $P < .01$).

Maps of T1, T2, and Trace(**D**) at four distinctive time points during development and at approximately the same anatomic level in a representative animal are shown in Figure 1. Corresponding anatomic maps of an adult cat are also shown. The time courses of the average values and the SDs of these parameters in various anatomic ROIs are shown in Figure 2. At birth, the orientationally averaged water diffusion coefficient (D_{oav} = Trace[**D**]/3) was higher than that in the adult in all brain regions (in newborns, D_{oav} was 1,000–1,350 μm^2/sec and, in adults, 600–750 μm^2/sec) but was still markedly lower than that in free solution (3,000 μm^2/sec at 37°C [2]).

The T1, T2, and Trace(**D**) maps were similar in the newborn brain. For all three parameters, the highest values were in the subcortical WM, followed by those in the corpus callosum and the internal capsule, with the lowest values in GM. T2 and Trace(**D**) show similar and chronologically parallel changes during development. The difference between WM and GM decreases markedly during the postnatal period and virtually disappears after the 5th week of life. The timing of this process varies in different WM regions, however. At 2 weeks, for example, on both T2 and Trace(**D**) maps, the subcortical WM is still brighter than GM, while the internal capsule is already isointense with GM. In the adult brain, all WM structures have essentially identical values for T2 and Trace(**D**) (Figs 1, 2). Initially, T1 shows an evolution similar to that of T2 and Trace(**D**), but the isointense phase in WM-to-GM contrast is followed by a further reduction of T1 in WM. This causes an inversion of WM-to-GM contrast (T1 of WM becomes shorter than T1 of GM), which is complete in all anatomic regions by the end of the 2nd month of life.

We first tested for correlations between parameters by using the entire data set, including data from all animals at all time points and all ROIs, in a single regression analysis (Fig 3). We found statistically significant correlations between Trace(**D**) and 1/T2 ($R^2 = 0.87$), 1/T1 and 1/T2 ($R^2 = 0.79$), and Trace(**D**) and 1/T1 ($R^2 = 0.76$). We repeated the tests for each individual ROI and found significant correlations between all parameters in all ROIs. For each correlation, we also determined whether the slope and intercept of the regression lines were significantly different in different ROIs. For the regression of Trace(**D**) versus 1/T2, there were no significant differences between ROIs, with the exception of the ROI in subcortical WM, for which both the slope and the intercept were significantly different from those of the other ROIs. For the regressions of Trace(**D**) versus 1/T1 and 1/T1 versus 1/T2, all WM ROIs differed significantly from the GM ROIs.

Phantom Study

The percent error of the imaging-measured T2 versus the spectroscopically-measured T2 in the phantoms was less than 5% for the entire range of T2 values measured in the animal's brain. We are confident, therefore, that our in vivo brain T2 measurements were accurate and reliable.

DISCUSSION

The main goals of this study were (*a*) to measure the orientationally averaged water diffusivity (Trace[**D**]/3) in the developing brain and (*b*) to assess whether this diffusion parameter can provide information that is not obtainable with conventional, relaxometry-based MR imaging. We found that Trace(**D**) dramatically changed in the maturing brain; however, the high degree of correlation between Trace(**D**) and the relaxation rates 1/T1 and 1/T2 suggests that little additional information can be obtained by measuring this diffusion parameter during normal brain development. Moreover, although T1-weighted images and T2-weighted images are thought to provide somewhat independent information in the clinical assessment of brain development, we found that the T1 and T2 relaxation rates were also highly correlated. We first discuss our relaxation and diffusion data in relation to data from the literature; then we propose possible biophysical explanations for our findings; finally, we describe clinically relevant aspects of our study.

Relaxation Measurements

To our knowledge, there have been no previous studies of the time course of changes in relaxation times during brain maturation in cats and few quantitative studies in other animal models (21) and

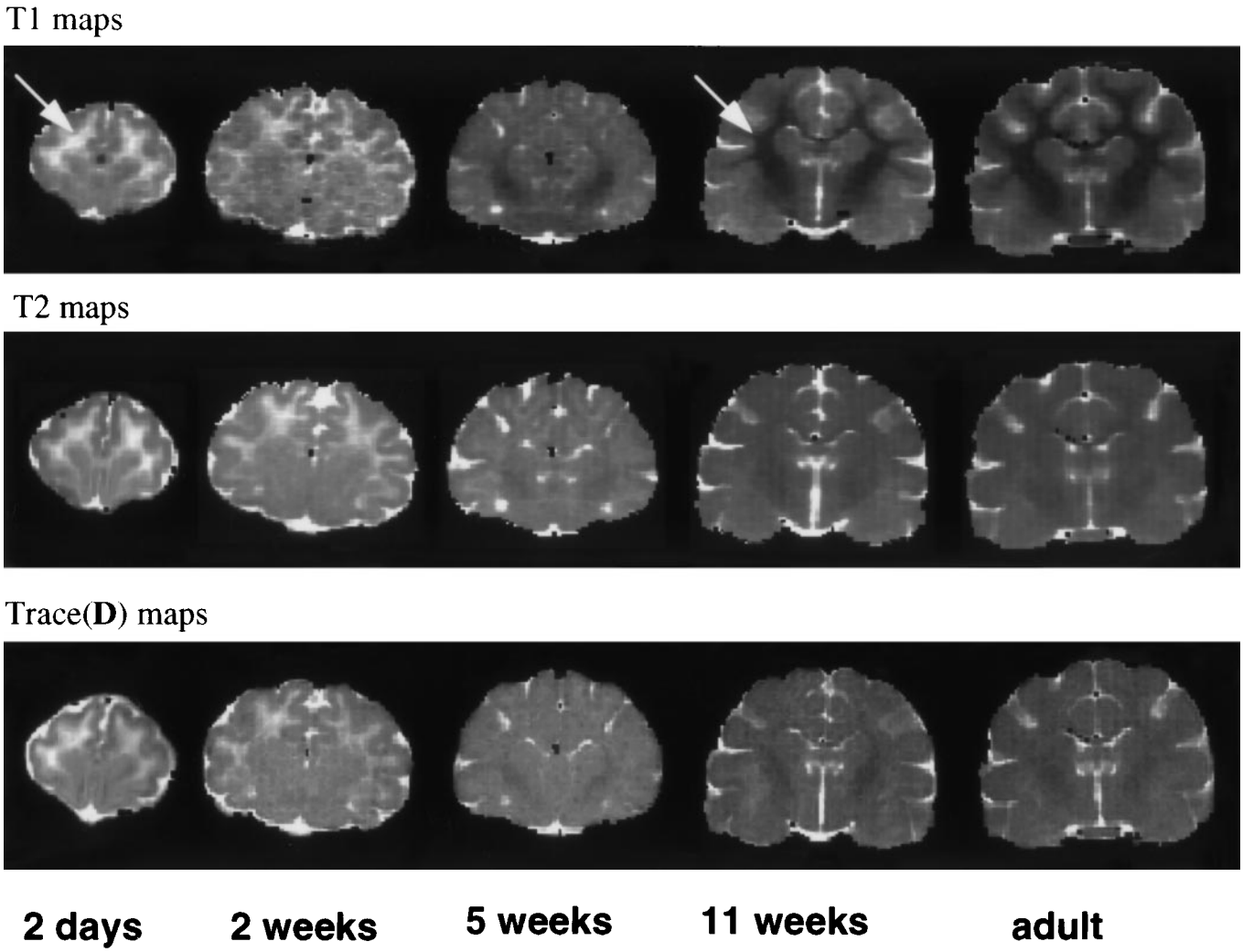

Figure 1. Changes in brain tissues during development as depicted on the maps of T1 (top), the long component of T2 (middle), and Trace(**D**) (bottom). Anatomically corresponding coronal sections acquired in the same representative kitten and in an adult cat are shown. Five relevant time points have been selected. The time courses of Trace(**D**) and T2 show clear similarities. In both cases, the highest values are observed in the newborn brain, where WM appears brighter than GM. During development, Trace(**D**) and T2 decrease in a parallel manner with a progressive reduction of the WM-to-GM contrast. In the adult brain, both Trace(**D**) and T2 have similar values in WM and GM. The time course of T1 partly resembles that of T2 and Trace(**D**) for the first 5 weeks, but, after the 5th week, there is a clearly visible inversion in the contrast between WM (arrows) and GM.

in humans (22–25). Our results contradict most of these previous results in two important aspects.

First, we found that both T1 and T2 were significantly longer in WM than in GM in the newborn brains, whereas previous investigators (22,24) found no T1 and T2 differences between subcortical WM and GM. Second, in the aforementioned studies (22–25), large differences between WM T2 and GM T2 in the adult brain were reported, but we found T2 to be almost the same in all mature brain tissues. It is unlikely that these discrepancies are related to interspecies differences, because both the general pattern of postnatal brain maturation and the structural and chemical features of the adult brain are similar in all mammals (12), although at birth the brain may be slightly more immature in cats than in humans. We attribute these discrepancies to the fact that most quantitative studies on brain maturation were performed in the early days of MR imaging and may have been affected by technical limitations (26). In particular, they were performed at very low field strength (0.15–0.35 T), and T2 was calculated from only two echoes. The accuracy of our T2 measurements is supported by the good agreement between the imaging-measured T2 and the spectroscopically-measured T2 in the phantoms. Our finding that mature WM and GM have similar T2 values is also in agreement with accurate relaxaometry studies (27,28) of the human brain in healthy adults.

Overall, our data indicate that T1 and T2 are similarly affected by the changes occurring in the maturing brain, with the exception of a much higher sensitivity of T1 to myelinization. The different sensitivity of T1 and T2 to myelinization can be explained in terms of the different effects of myelin-associated water on T1 and T2. It has been shown (29) that T2 in WM has two distinct components: a long T2 component (about 70–90 msec at 1.5 T), which has been attributed to axonal and extracellular water, and a short T2

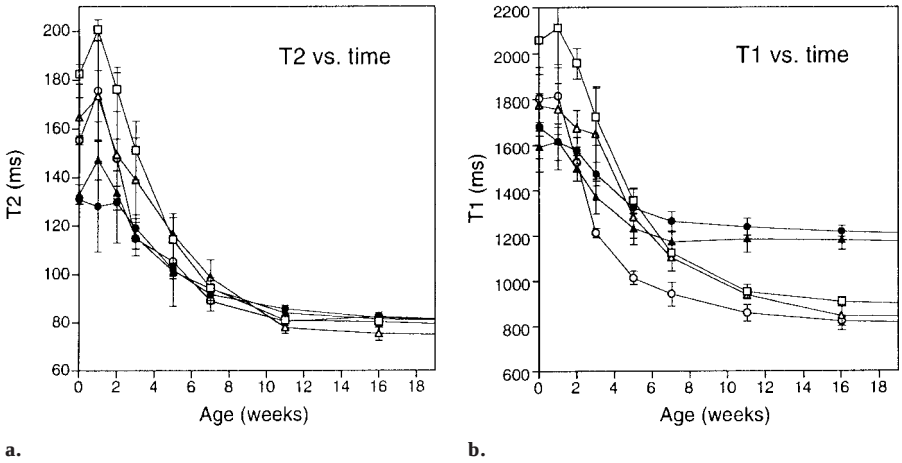

Figure 2. Graphs show the time course of changes in mean values measured in four kittens for **(a)** the long component of T2, **(b)** T1, and **(c)** Trace(**D**) for ROIs in subcortical WM (□), the internal capsule (○), the corpus callosum (△), the cortex (●), and the caudate nucleus (▲). Error bars = SDs, *ms* = milliseconds, *s* = seconds. The time course of the changes shown in **a** and **c** are similar for all ROIs. The changes shown in **b** show two patterns for WM and GM ROIs.

component (<20 msec at 1.5 T), which has been attributed to myelin water. Because our T2 relaxation curves were calculated from echoes acquired at relatively long echo times, the measured T2 corresponds to the long T2 component of axonal and extracellular water and is unaffected by myelin water. T2 in WM has two distinct components because, in the time scale of typical T2 values in brain tissues, there is no substantial exchange between myelin water and water in other compartments. In the time scale of typical T1 values, however, myelin water can diffuse across axonal and myelin membranes and interact with water molecules in other compartments. Therefore, signal decay due to T1 relaxation is monoexponential in myelinated WM, and myelin water produces T1 shortening in WM as myelinization progresses (30).

Clinical Implications of Relaxation Findings

We mentioned that, to our knowledge, there are no reliable measurements of T1 and, in particular, T2 in the developing human brain. There are, however, several advantages that would originate from knowledge of the time course of relaxation parameters in the developing brain.

First, the acquisition of "weighted" (eg, T1-weighted, T2-weighted) images instead of T1 and T2 maps for diagnostic purposes implies that one must rely on the evaluation of differences in contrast between brain regions rather than on a quantitative comparison with normative values for the population. Our data show that large changes in the relaxation properties tend to occur simultaneously in various brain regions and in different brain tissues. For this reason, if we are interested in staging brain maturation, the acquisition of weighted images is intrinsically less sensitive than the acquisition of relaxation parameters, because substantial changes in relaxation parameters may be accompanied by only minor changes in image contrast.

Second, the analysis of relaxation parameters would facilitate a more specific understanding of the biophysical determinants of the MR signal than would inspection of image contrast on weighted images. For example, we found that T1 and the long component of T2 provide similar information on brain maturation, with the exception of a clearly different sensitivity to myelinization.

Third, better knowledge of the behavior of the relaxation parameters in the developing brain could help in the design of more specific and efficient weighted imaging protocols. For example, a standard approach to monitoring myelinization in pediatric neuroradiology is to rely on T1-weighted images during the first 6 months of life and on T2-weighted images thereafter. Changes in the contrast between GM and WM on T1-weighted images have been attributed to the effect of increased myelin, whereas changes on T2-weighted images have been attributed to secondary maturation processes of myelin, such as tightening of the myelin spiral around the axon (1). Our results suggest that the WM-to-GM contrast changes observed on long repetition time and long echo time T2-weighted images obtained at the late stage of brain development are not dependent on changes in the long T2 component. As shown in Figure 4, notable changes in contrast on T2-weighted images occur when no additional changes can be appreciated on the maps of the long T2 component.

When the long T2 component as a source of these contrast changes is excluded, three other factors remain to be considered: proton density of the long T2 component, proton density of the short T2 component, and the short T2 component itself. Although further work is necessary to identify which of these factors is primarily responsible, our data suggest that images acquired with a long repetition time and a relatively short echo time (25–30 msec) should provide the same information on myelinization progression as that provided by long echo time, long repetition time images, with the advantage of a better signal-to-noise ratio.

Measurements of the Trace of the Diffusion Tensor

To our knowledge, this is the first study in which changes in orientationally averaged water diffusivity were measured in different anatomic regions during the entire course of postnatal brain development. Because previous studies of brain maturation used diffusion-weighted images (31,32) or apparent-diffusion-coefficient measurements in one (6) or two (4,5) directions, the results of those studies are not directly comparable with our results. Moreover, none of the authors of these previous studies reported data on GM, and the variability of apparent-diffusion-coefficient values in WM is generally high, probably because of differences in the relative directions of the fibers and the applied diffusion gradients, which were controlled for in our study.

Our finding that Trace(**D**) was significantly higher in the immature brain than in the adult brain in all anatomic regions is in agreement with and extends the results of Sakuma et al (4), Toft et al (6), and Neil et al (33). In addition, we found that Trace(**D**) in the newborn is statistically different in different anatomic regions, which is in agreement with previous findings (34) of reported differences in D_{oav} between GM and subcortical WM in newborn piglets. Our data show that these regional differences are progressively less noticeable during maturation and disappear almost completely in the adult brain.

We found a high degree of correlation between Trace(**D**) and 1/T2 during development. Moreover, the regression lines of Trace(**D**) versus 1/T2 in different ROIs were virtually superimposed, with no significant differences in either slope or intercept. This result is important because it signifies that in all brain regions and at all time points D_{oav} and T2 respond similarly to the various physicochemical and histologic changes that occur during tissue maturation.

The situation is markedly different in brain ischemia and stroke, where 1/T2 and Trace(**D**) are not strongly correlated. In fact, in brain ischemia, as well as in the early stage of an infarct, there is a rapid decrease in D_{oav} (35–37), with no detectable changes on either T2-weighted images (3) or T2 maps (38). Moreover, when vasogenic edema develops at a later stage, water diffusivity in the infarcted tissue remains low, while T2-weighted signal intensity increases. Finally, during chronic infarct progression, cellular lysis causes a dramatic reelevation of the diffusion coefficient but does not markedly affect the T2-weighted imaging results (39).

An understanding of the causes of the different behavior of diffusion and relaxation parameters in ischemia and development, as well as the unequivocal determination of a relationship between our diffusion results and specific structural or chemical features of the developing brain, is not simple. The MR imaging–measured water diffusivity is indeed a composite measure that reflects the contribution of multiple and heterogeneous microscopic tissue compartments. Recent analytic studies (40) and numeric simulations (41,42) of simplified models, however, have been helpful in elucidating the relative contribution of some important factors, such as the geometry, size, and intrinsic water diffusivity of the cellular and extracellular compartments. In the case of ischemia, for instance, most studies suggest that the decreased water diffusivity as measured with MR imaging is essentially related to an increased tortuosity and diminished volume fraction of the "fast-diffusivity" extracellular compartment.

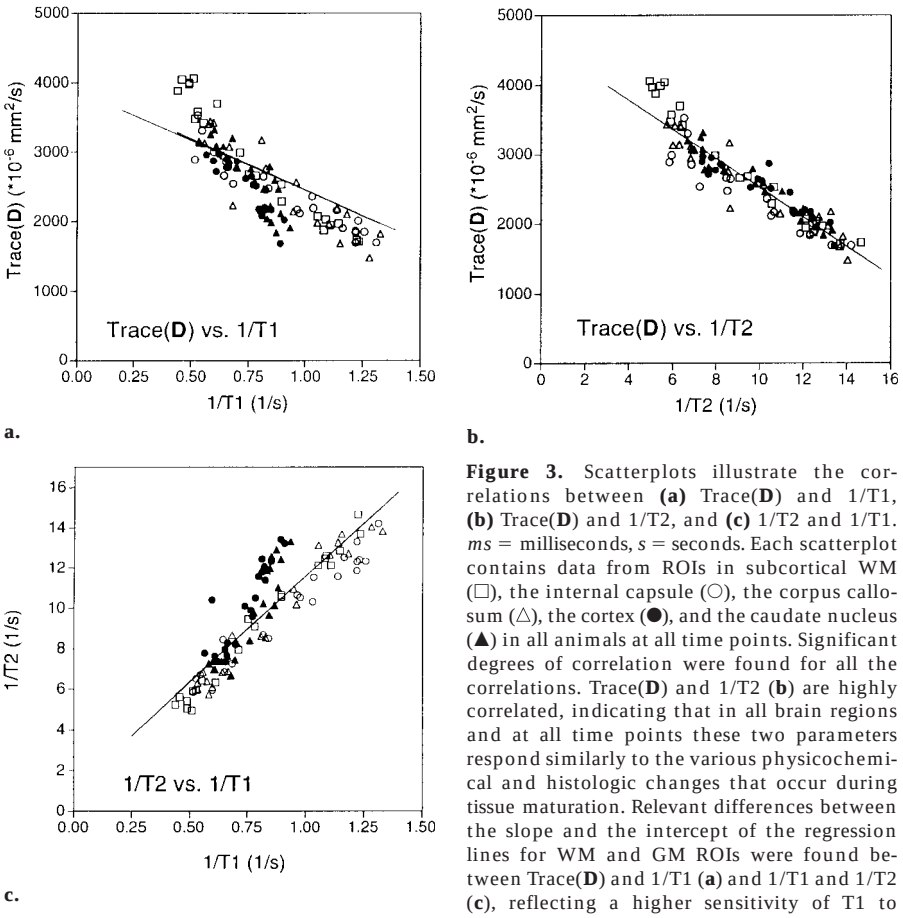

Figure 3. Scatterplots illustrate the correlations between **(a)** Trace(**D**) and 1/T1, **(b)** Trace(**D**) and 1/T2, and **(c)** 1/T2 and 1/T1. *ms* = milliseconds, *s* = seconds. Each scatterplot contains data from ROIs in subcortical WM (□), the internal capsule (○), the corpus callosum (△), the cortex (●), and the caudate nucleus (▲) in all animals at all time points. Significant degrees of correlation were found for all the correlations. Trace(**D**) and 1/T2 (**b**) are highly correlated, indicating that in all brain regions and at all time points these two parameters respond similarly to the various physicochemical and histologic changes that occur during tissue maturation. Relevant differences between the slope and the intercept of the regression lines for WM and GM ROIs were found between Trace(**D**) and 1/T1 (**a**) and 1/T1 and 1/T2 (**c**), reflecting a higher sensitivity of T1 to myelin.

To better clarify the microstructural determinants of our results, we analyzed our data by using the model recently proposed by Latour et al (40), which is applicable given our limit of long diffusion time and weak diffusion pulses. If we assume that the concentration of water is the same in both extracellular and intracellular compartments, then this model consists of an equation that relates the MR imaging–measured D_{oav} to the extracellular diffusivity D_{ext}, the volume fraction of the extracellular space α, and the effective diffusivity of the cellular compartment $D_{effcell}$. Because our MR measurement was insufficient to determine all the parameters of the model, we integrated our MR imaging data with data from iontophoretic measurements (43–45), which provide selective information on the diffusion properties of the extracellular space. Unfortunately, iontophoretic measurements are available only in rats; therefore, for the sake of this discussion, we shall assume that feline brain development is sufficiently similar to that of rats. A detailed description of our approach is presented in the Appendix; here we present only the conclusion of our analysis.

Our diffusion MR imaging experiments show that between birth and adulthood, D_{oav} in GM decreases from 1,000 to 700 μm^2/sec—a 30% decrease, which is of the same magnitude as that observed after ischemia (46). By using the values of α and D_{ext} obtained from the iontophoretic measurements of Lehmenkuhler et al (44), we calculated that $D_{effcell}$ changed from 650 μm^2/sec at birth to 420 μm^2/sec in adulthood, a decrease of about 35%. We used the same method to analyze the results in models of ischemia. By combining the iontophoretic data of Vorisek and Sykova (47) with diffusion MR imaging measurements of ischemia in cats (46), we found that $D_{effcell}$ does not decrease after ischemia and shows a modest change from 380 μm^2/sec in the nonischemic brain to 440 μm^2/sec during ischemia.

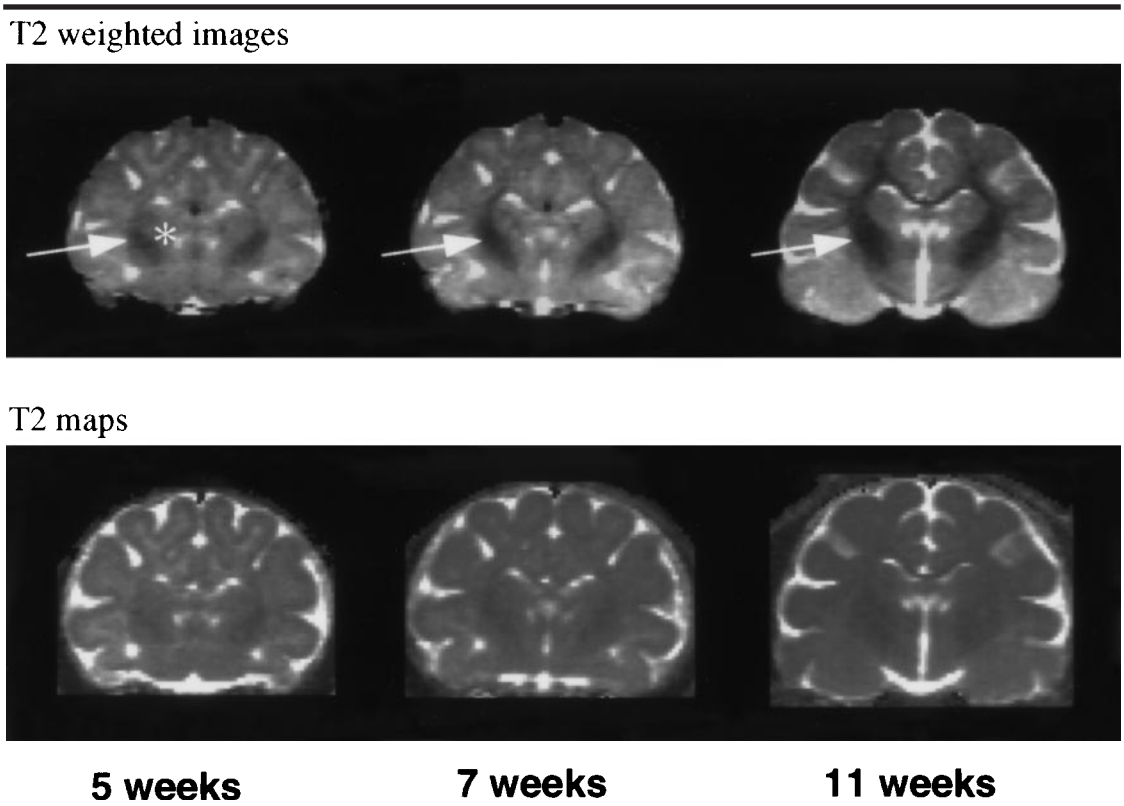

Figure 4. Late phase of myelinization in the internal capsule. Top: On T2-weighted MR images (5,000/100), the internal capsule (arrows) shows a progressive reduction in signal intensity as compared with GM structures such as the head of the caudate nucleus (∗). Bottom: On maps of the long component of T2, there are minimal differences between the internal capsule and GM at all time points, which indicates that the contrast changes visible on T2-weighted images (top) are unrelated to changes in the long component of T2. This finding implies that for the evaluation of the later phase of myelinization in children, MR images acquired with a long repetition time and a relative short echo time (eg, 30 msec) would provide the same tissue contrast as do images acquired with a long echo time; the former would, however, have the advantage of a better signal-to-noise ratio.

We cannot expect the numeric values in the preceding paragraph to be accurate because the MR imaging and iontophoretic diffusion data were obtained in different species. In qualitative terms, however, the results of this analysis suggest that changes in Trace(**D**) during ischemia are primarily caused by changes in the diffusion properties of the extracellular space, whereas the changes during development are primarily caused by changes in the effective diffusivity of the cellular compartment.

We identify two main biologic events that could contribute to modifications in the diffusivity of the cellular compartment and consequently affect Trace(**D**) during development: (*a*) an increased concentration of macromolecules (48) and (*b*) a greater membrane surface–to–cell volume ratio caused by the proliferation of processes and organelles (49). Another possible factor would be a change in cell membrane permeability; however, this is difficult to asses experimentally, and we are not aware of any studies in which this possibility was investigated during brain development.

The results of our analysis also may explain why the T2 changes parallel the Trace(**D**) changes in development but not in ischemia. T2 relaxation is caused by fluctuations of the local magnetic field (50). These fluctuations are caused by the relative motion of the spins and the sources of local fields represented by unpaired electrons and other magnetic nuclei. Changes in the viscosity of the medium, which determine the variation in the rate of relative motion, as well as changes in the chemical composition of the medium, which affect the concentration of sources of the local field, are expected to affect T2. Of interest, the same cellular events that we suggested may cause the changes in Trace(**D**) during development, such as increased concentration of macromolecules and membranes, also modify the chemical composition and viscosity of the tissue, which could theoretically affect T2. In addition, experimental works (51) have shown that membranes and macromolecules shorten T2.

During acute ischemia, however, there are no such changes in tissue composition. In essence, no ''new material'' is created that could shorten T2; there is a change in water compartmentalization only. The resultant increased tortuosity of the extracellular compartment has a marked effect on water diffusivity but does not substantially affect T2, because it acts over large distances as compared with the nearest-neighbor distances that dominate T2 relaxation.

In conclusion, we believe that a complete understanding of the mechanisms of water diffusion and relaxation in tissues necessitates additional theoretic and experimental work. However, the results of our analysis provide a plausible explanation of how our findings are related to different tissue microstructural changes that occur in development and ischemia and suggest that the determinants of the reduced Trace(**D**) in development may differ profoundly from those in ischemia.

Clinical Implications of Diffusion Findings

If confirmed with studies in healthy human subjects, our finding of a surprising similarity in the information provided by the long T2 component and Trace(**D**) could discourage the use of diffusion MR sequences to assess brain development. We believe, however, that this conclusion is erroneous at this time for two reasons.

First, we have no assurance that analogous findings would be confirmed in pathologic conditions. Brain ischemia and stroke are clear examples of diseases where average diffusivity and T2 behave differently. Because almost no pediatric diseases have been investigated with quantitative diffusion MR imaging, we should first obtain sufficient diffusion data on pathologic conditions before concluding that the average water diffusivity provides no additional useful information in pediatric radiology.

Second, Trace(**D**) is not the only parameter that we can compute in a quantitative study of water diffusion in tissues. Other diffusion parameters such as diffusion anisotropy and the principal direction of diffusion may be informative even if Trace(**D**) is not. In the normal adult brain, it has already been demonstrated (11) that diffusion anisotropy provides anatomic and structural data that are unavailable from conventional MR imaging. Moreover, results of preliminary studies (52) indicate that in brain development, diffusion anisotropy and relaxation times show different behaviors in both WM and GM regions.

Practical applications: Various physical parameters that could potentially provide different information on the structure, chemical composition, and metabolic state of the brain can be measured with MR imaging. Our quantitative assessment of T1, T2, and Trace(**D**) during normal brain development has been useful for the determination of the extent to which different parameters provide independent information, as well as for the attempt to understand the biologic correlates of such changes. We believe that a quantitative approach would be particularly advantageous in pediatric neuroradiology because, in the developing brain, weighted imaging has the intrinsic limitation of no internal reference that can be considered to be invariant. We also believe that the increased availability of fast MR imaging sequences will greatly simplify the task of performing similar studies in the clinical setting.

APPENDIX

The Latour effective medium theory describes the diffusivity of small molecules in a system consisting of a suspension of spherical cells. The theory leads to the following equation:

$$\left(\frac{D_{\text{eff}}c_{\text{eff}} - D_1 c_{\text{int}}}{D_{\text{ext}}c_{\text{ext}} - D_1 c_{\text{int}}}\right)\left(\frac{D_{\text{ext}}c_{\text{ext}}}{D_{\text{eff}}c_{\text{eff}}}\right)^{1/3} = \alpha, \quad \text{(A1)}$$

where α is the volume fraction of the suspension occupied by the external medium; D_{eff} is the effective diffusivity in the system as a whole and characterizes the diffusion properties of the system on a size scale that is large compared with the size of the cells and the separation between them; D_{ext} is the diffusivity in the external medium and is the expected result of a diffusivity measurement in a cell-free system; c_{ext} is the fractional concentration of the diffusing molecules in the external medium; c_{int} is the fractional concentration of the diffusing molecules inside the cells; c_{eff} is the average concentration of the diffusing molecules in the system as a whole and is related to the other parameters by

$$c_{\text{eff}} = \alpha c_{\text{ext}} + (1 - \alpha)c_{\text{int}}; \quad \text{(A2)}$$

and D_1 is the effective diffusivity in the cellular compartment, including the cell membrane. D_1 is defined by

$$D_1 = \frac{\kappa a D_{\text{int}}}{\kappa a + D_{\text{int}}c_{\text{int}}}, \quad \text{(A3)}$$

where κ is the permeability of the membrane that separates the cells from the external medium, a is the radius of the cells, and D_{int} is the diffusivity of the intracellular medium.

If we model neurons as spherical cells suspended in an extracellular medium, Equations (A1)–(A3) can describe both ion tracer measurements and MR diffusion measurements. We first apply the equations to ion tracer experiments. Analysis of data from ion tracer measurements yields values for three parameters: the volume fraction α, the tortuosity λ, and the nonspecific uptake k (see reference 43). The tortuosity λ is related to D_{M}^{t}, the measured diffusivity of the tracer in the brain, by

$$D_{\text{M}}^{\text{t}} = \frac{D_0^{\text{t}}}{\lambda^2}, \quad \text{(A4)}$$

where D_0^{t} is the diffusivity of the tracer in the calibration solution. The ion tracer experiments actually measure D_{M}^{t}, but the result quoted is λ as defined by Equation (A4). Note that λ depends on the viscosity of the extracellular medium, as well as on the geometry of the extracellular space. We can use Equation (A1) to relate $D_{\text{ext}}^{\text{t}}$ to D_0^{t} and therefore separate out the effect of the viscosity of the medium from the effect of geometry. If the nonspecific uptake is sufficiently small, $c_{\text{int}}^{\text{t}}$ is 0 and Equation (A1) reduces to

$$\frac{D_{\text{eff}}}{D_{\text{ext}}} = \sqrt{\alpha}. \quad \text{(A5)}$$

By equating D_{eff} in Equation (A5) to D_{M}^{t} in Equation (A4), we find that

$$D_{\text{ext}}^{\text{t}} = \frac{D_0^{\text{t}}}{\lambda^2/\sqrt{\alpha}}. \quad \text{(A6)}$$

To the extent that λ is the same for any molecule, Equation (A6) also applies to water molecules:

$$D_{\text{ext}}^{\text{w}} = \frac{D_0^{\text{w}}}{\lambda^2\sqrt{\alpha}}, \quad \text{(A7)}$$

where the superscript "w" denotes water.

We can also apply Equation (A1) to the diffusion MR imaging measurements. In this case, D_{eff} becomes D_{oav}, the MR imaging–measured diffusion constant, and D_1 becomes D_{effcell}. If we assume that c_{int}

TABLE A1
Changes in Diffusivity during Development and in Acute Ischemia

Cause of Change	α	λ	D_{oav} (μm^2/sec)	$D_{\text{ext}}^{\text{w}}$ (μm^2/sec)	D_{effcell} (μm^2/sec)
Developmental					
Newborn	0.36*	1.65*	1,000	1,800	650
Adult	0.20*	1.63*	700	2,500	420
Ischemic					
Normal	0.23†	1.5†	730‡	2,780	380
Ischemia	0.06†	2.0†	530‡	3,060	440

* Source, reference 44.
† Source, reference 47.
‡ Source, reference 46.

equals c_{ext}, we find that

$$D_{effcell} = D^{w}_{ext}\left[\frac{\alpha\left\langle\left(\frac{D_{oav}}{D^{w}_{ext}}\right)^{1/3}\right\rangle - \left\langle\frac{D_{oav}}{D^{w}_{ext}}\right\rangle}{\alpha\left\langle\left(\frac{D_{oav}}{D^{w}_{ext}}\right)^{1/3}\right\rangle - 1}\right]. \quad \text{(A8)}$$

From Equation (A3), we see that the effective diffusivity $D_{effcell}$ is dependent on the cell radius a, membrane permeability κ, and intracellular water diffusivity D^{w}_{int}. D^{w}_{int}, in turn, is itself a composite parameter; it is not the bulk diffusivity of the intracellular medium but rather is dependent on the presence and characteristics of organelles and other intracellular constituents.

In conclusion, MR imaging measurements in the long-diffusion, weak-diffusion weighting limit give no information about the values of D^{w}_{ext} and $D_{effcell}$ individually. However, if we use the values of λ and α from the ion tracer measurements and D_{oav} from the diffusion measurements, Equations (A7) and (A8) can be used to compute D^{w}_{ext} and $D_{effcell}$. The results for development and ischemia are given in Table A1.

Acknowledgments: The authors thank Tory Hampshire, MD, and the personnel of Building 28 at the National Institutes of Health for their assistance and suggestions in the use of the animals. The authors also thank Josef Vymazal, MD, and Jeff Bulte, MD, for providing the samples used in the T2 spectroscopic experiment. The skillful editing of Devera G. Schoenberg, MS, is also appreciated.

References

1. Barkovich AJ. Pediatric neuroimaging. New York, NY: Raven, 1995; 20–36.
2. Le Bihan D. Molecular diffusion nuclear magnetic resonance imaging. Magn Reson Q 1991; 7:1–30.
3. Moseley ME, Kucharczyk J, Mintorovitch J, et al. Diffusion-weighted MR imaging of acute stroke: correlation with T2-weighted and magnetic susceptibility–enhanced MR imaging in cats. AJNR 1990; 11:423–429.
4. Sakuma H, Nomura Y, Takeda K, et al. Adult and neonatal human brain: diffusional anisotropy and myelination with diffusion-weighted MR imaging. Radiology 1991; 180:229–233.
5. Nomura Y, Sakuma H, Takeda K, et al. Diffusional anisotropy of the human brain assessed with diffusion-weighted MR: relation with normal brain development and aging. AJNR 1994; 15:231–238.
6. Toft PB, Leth H, Peitersen B, Lou HC, Thomsen C. The apparent diffusion coefficient of water in gray and white matter of the infant brain. J Comput Assist Tomogr 1996; 20:1006–1011.
7. Pierpaoli C, Basser PJ. Toward a quantitative assessment of diffusion anisotropy. Magn Reson Med 1996; 36:893–906. [Erratum: Magn Reson Med 1997; 37:972.]
8. Basser PJ, Mattiello J, Le Bihan D. MR diffusion tensor spectroscopy and imaging. Biophys J 1994; 66:259–267.
9. van Gelderen P, de Vleeschouwer MH, DesPres D, et al. Water diffusion and acute stroke. Magn Reson Med 1994; 31:154–163.
10. Liu G, van Gelderen P, Duyn J, Moonen CT. Single-shot diffusion MRI of human brain on a conventional clinical instrument. Magn Reson Med 1996; 35:671–677.
11. Pierpaoli C, Jezzard P, Basser PJ, Barnett A, Di Chiro G. Diffusion tensor MR imaging of the human brain. Radiology 1996; 201: 637–648.
12. Dobbing J, Sands J. Quantitative growth and development of human brain. Arch Dis Child 1973; 48:757–767.
13. Volpe JJ. Neurology of the newborn. Philadelphia, Pa: Saunders, 1987; 79–84.
14. Hildebrand C, Skoglund S. Calibre spectra of some fibre tracts in the feline central nervous system during postnatal development. Acta Physiol Scand Suppl 1971; 364: 5–41.
15. Jezzard P, Barnett A, Pierpaoli C. Characterization of and correction for eddy current artifacts in echo planar diffusion imaging. Magn Reson Med 1998; 39:801–812.
16. Mattiello J, Basser PJ, Le Bihan D. The b matrix in diffusion tensor echo-planar imaging. Magn Reson Med 1997; 37:292–300.
17. Basser PJ, Mattiello J, Le Bihan D. Estimation of the effective self-diffusion tensor from the NMR spin echo. J Magn Reson B 1994; 103:247–254.
18. Mulkern RV, Wong ST, Jakab P, et al. CPMG imaging sequences for high field in vivo transverse relaxation studies. Magn Reson Med 1990; 16:67–79.
19. Bevington PR. Data reduction and error analysis for the physical sciences. New York, NY: McGraw-Hill, 1969; 336.
20. Tofts PS, du Boulay EP. Towards quantitative measurements of relaxation times and other parameters in the brain. Neuroradiology 1990; 32:407–415.
21. Miot-Noirault E, Barantin L, Akoka S, Le Pape A. T2 relaxation time as a marker of brain myelination: experimental MR study in two neonatal animal models. J Neurosci Methods 1997; 72:5–14.
22. Holland BA, Haas DK, Norman D, Brant-Zawadzki M, Newton TH. MRI of normal brain maturation. AJNR 1986; 7:201–208.
23. Masumura M. Proton relaxation time of immature brain. II. In vivo measurement of proton relaxation time (T1 and T2) in pediatric brain by MRI. Childs Nerv Syst 1987; 3:6–11.
24. Baierl P, Forster C, Fendel H, Naegele M, Fink U, Kenn W. Magnetic resonance imaging of normal and pathological white matter maturation. Pediatr Radiol 1988; 18:183–189.
25. Ono J, Kodaka R, Imai K. Evaluation of myelination by means of the T2 value on magnetic resonance imaging. Brain Dev 1993; 15:422–438.
26. Bottomley PA, Hardy CJ, Argersinger RE, Allen-Moore G. A review of 1H nuclear magnetic resonance relaxation in pathology: are T1 and T2 diagnostic? Med Phys 1987; 14:1–37.
27. Drayer B, Burger P, Darwin R, et al. MRI of brain iron. AJR 1986; 147:103–110.
28. Wehrli FW, MacFall JR, Shutts D, Breger R, Herfkens RJ. Mechanisms of contrast in NMR imaging. J Comput Assist Tomogr 1984; 8:369–380.
29. Whittall KP, MacKay AL, Graeb DA, et al. In vivo measurement of T2 distributions and water contents in normal human brain. Magn Reson Med 1997; 37:34–43.
30. Koenig SH, Brown RD III, Spiller M, Lundbom N. Relaxometry of brain: why white matter appears bright in MRI. Magn Reson Med 1990; 14:482–495.
31. Rutherford MA, Cowan FM, Manzur AY, et al. MR imaging of anisotropically restricted diffusion in the brain of neonates and infants. J Comput Assist Tomogr 1991; 15:188–198.
32. Wimberger DM, Roberts TP, Barkovich AJ, et al. Identification of "premyelination" by diffusion-weighted MRI. J Comput Assist Tomogr 1995; 19:28–33.
33. Neil JJ, McKinstry RC, Snyder AZ, Lee BCP, Conturo TE. Quantitative measurement of brain water apparent diffusion coefficient in healthy full-term neonates (abstr). In: Proceedings of the Fourth Meeting of the International Society for Magnetic Resonance in Medicine. Berkeley, Calif: International Society for Magnetic Resonance in Medicine, 1996; 599.
34. Thornton JS, Ordidge RJ, Penrice J, et al. Anisotropic water diffusion in white and gray matter of the neonatal piglet brain before and after transient hypoxia-ischaemia. Magn Reson Imaging 1997; 15:433–440.
35. Davis D, Ulatowski J, Eleff S, et al. Rapid monitoring of changes in water diffusion coefficients during reversible ischemia in cat and rat brain. Magn Reson Med 1994; 31:454–460.
36. Decanniere C, Eleff S, Davis D, van Zijl PC. Correlation of rapid changes in the average water diffusion constant and the concentrations of lactate and ATP breakdown products during global ischemia in cat brain. Magn Reson Med 1995; 34:343–352.
37. Pierpaoli C, Alger JR, Righini A, et al. High temporal resolution diffusion MR imaging of global cerebral ischemia and reperfusion. J Cereb Blood Flow Metab 1996; 16:892–905.
38. Hoehn-Berlage M, Eis M, Back T, Kohno K, Yamashita K. Changes of relaxation times (T1, T2) and apparent diffusion coefficient after permanent middle cerebral artery occlusion in the rat: temporal evolution, regional extent, and comparison with histology. Magn Reson Med 1995; 34:824–834.
39. Pierpaoli C, Righini A, Linfante I, et al. Histopathologic correlates of abnormal water diffusion in cerebral ischemia: diffusion-weighted MR imaging and light and electron microscopic study. Radiology 1993; 189:439–448.
40. Latour LL, Svoboda K, Mitra PP, Sotak CH. Time-dependent diffusion of water in a biological model system. Proc Natl Acad Sci USA 1994; 28:107–116.
41. Szafer A, Zhong J, Gore JC. Theoretical model for water diffusion in tissues. Magn Reson Med 1995; 33:697–712.
42. Stanisz GJ, Szafer A, Wright GA, Henkelman RM. An analytical model of restricted diffusion in bovine optic nerve. Magn Reson Med 1997; 37:103–111.
43. Nicholson C, Phillips JM. Ion diffusion modified by tortuosity and volume fraction in the extracellular microenvironment of the rat cerebellum. J Physiol (Lond) 1981; 321:225–257.
44. Lehmenkuhler A, Sykova E, Svoboda J,

Zilles K, Nicholson C. Extracellular space parameters in the rat neocortex and subcortical white matter during postnatal development determined by diffusion analysis. Neuroscience 1993; 55:339–351.
45. Sykova E. Extracellular space volume and geometry of the rat brain after ischemia and central injury. Adv Neurol 1997; 73: 121–135.
46. Pierpaoli C, Baratti C, Jezzard P. Fast tensor imaging of water diffusion changes in gray and white matter following cardiac arrest in cats (abstr). In: Proceedings of the Fourth Meeting of the International Society for Magnetic Resonance in Medicine. Berkeley, Calif: International Society for Magnetic Resonance in Medicine, 1996; 314.
47. Vorisek I, Sykova E. Ischemia-induced changes in the extracellular space diffusion parameters, K+, and pH in the developing rat cortex and corpus callosum. J Cereb Blood Flow Metab 1997; 17:191–203.
48. Tower DB, Bourke RS. Fluid compartmentation and electrolytes of cat cerebral cortex in vitro. III. Ontogenetic and comparative aspects. J Neurochem 1966; 13:1119–1137.
49. Caley DW. Differentiation of the neural elements of the cerebral cortex in the rat. UCLA Forum Med Sci 1971; 14:73–102.
50. Abragam A. Principles of nuclear magnetism. London, England: Oxford University Press, 1961.
51. Sullivan SG, Stern A, Rosenthal JS, Minkoff LA, Winston A. NMR water-proton spin-lattice relaxation time of human red blood cells and red blood cell suspensions. FEBS Lett 1988; 234:349–352.
52. Baratti C, Barnett A, Pierpaoli C. Comparative MRI study of brain maturation using T1, T2, and the diffusion tensor. (abstr). In: Proceedings of the Fifth Meeting of the International Society for Magnetic Resonance in Medicine. Berkeley, Calif: International Society for Magnetic Resonance in Medicine, 1997; 504.